TABLE OF CONTENTS (TOC)

Thickness-Dependent Wrinkling of PDMS Films for Programmable Mechanochromic Responses

Zhiwei Li, Yun Liu, Melinda Marin, and Yadong Yin*

Department of Chemistry, University of California, Riverside, CA 92521, United States

E-mail: yadong.yin@ucr.edu

Page Numbers. The font is ArialMT 16 (automatically inserted by the publisher)

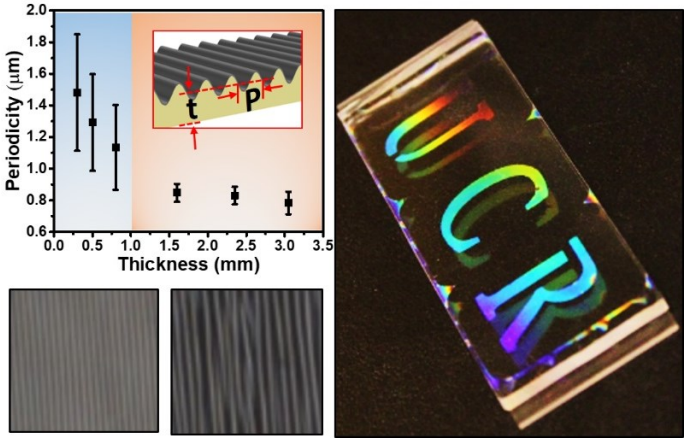

This work reveals the thickness dependence of the wrinkling behaviors of plasma-treated PDMS films. For thick films, the wrinkles can be predicted by the classic nonlinear finite mechanics, giving rise to brilliant structural colors. For thin films, the wrinkles are large and random. These observations provide new opportunities for understanding the wrinkling mechanics and have promising applications in smart optical materials.

Nano Res (automatically inserted by the publisher)
DOI (automatically inserted by the publisher)
Research Article Please choose one

Thickness-Dependent Wrinkling of PDMS Films for Programmable Mechanochromic Responses

Zhiwei Li, Yun Liu, Melinda Marin, and Yadong Yin(✉)

Department of Chemistry, University of California, Riverside, CA 92521, United States

E-mail: yadong.yin@ucr.edu

ABSTRACT

We report a remarkable thickness-dependent wrinkling behavior of oxygen plasma-treated polydimethylsiloxane PDMS films, in which an energy barrier separates the wrinkling mechanics into two regimes. For thick films, the film wrinkles with a constant periodicity which can be precisely predicted by the classic nonlinear finite mechanics. Reducing the film thickness below 1 mm leads to nonuniform wrinkles with an increasing periodicity which gives rise to random scattering and transparency changes under mechanical strains. By tuning the film thickness, we were able to control both the quality and size of the periodic wrinkles and further design mechanochromic devices featuring brilliant structural colors and programmable colorimetric responses. This work sheds light on the fundamental understanding of the wrinkling mechanics of bilayer systems and their intriguing mechanochromic applications.

KEYWORDS

wrinkle, PDMS, structural colors, mechanochromic, thickness-dependent

1 Introduction

Wrinkles on bilayer films with mechanical modulus contrast under mechanical or thermal perturbations were recognized in 1998 in the study of elastomer polymer-supported metal films.[1] Before that, wrinkles were regarded as mechanical failure and many efforts had been made to avoid the wrinkle formations. Subsequent studies revealed that wrinkles, generally formed on a thin rigid layer with high elastic modulus, were universal characteristics of many bi-layered structures, such as metal,[2-4] semiconductor,[5-8] C,[9-12] polystyrene,[13-16] and oxides on PDMS films.[17-22] It was then realized that this classic mechanical behavior could be carefully controlled and intentionally engineered into micro- or nanoscale with well-defined geometries and complex structures.[23] Together with the transparent characteristics of the elastomer, these unique wrinkling behaviors have been explored for various applications in stretchable electronics,[24] optics,[20,

21, 25-28] anti-counterfeiting,[29] and engineering mechanics.[9, 13, 30]

For many years, the semi-linear deformation mechanics is regarded as a fundamental description of the wrinkling process. It predicts that the periodicity of wrinkles is determined by the thickness of the top rigid layer and the elastic modulus ratio between the rigid layer and the bottom elastic substrate.[31-38] In a systematic study of stretching instability of Si ribbons-bonded PDMS films, a nonlinear finite mechanics was proposed by minimizing the perturbation energy.[6] In contrast to the semi-linear mechanics, the nonlinear finite mechanic takes the effects of strain on the periodicity (P) and amplitude (A) of wavy deformation into consideration. However, these mechanics fail again to investigate the effects of substrate thickness as it treats the substrate as a semi-infinite solid film and applies an infinite boundary condition to the perturbation. Albeit extensive experimental studies of various bilayer structures, the importance of substrate thickness has never been recognized in previous literature. Most reported methods generally produce wrinkles of large periodicity (several micrometers) or wrinkles with only short-range orders, which are found to be independent of the substrate thickness. As the optical performances of wrinkled bilayers are highly dependent on the wrinkle quality and size, it is therefore believed that the potentials of these unique wrinkling bilayer films have not been fully exploited. Herein, we reveal the significant impact of the thickness of the PDMS base films on both the periodicity and quality of the wrinkles formed under mechanical strains. This new understanding further enables the fabrication of various mechanochromic films with bright structural colors and pre-designed colorimetric responses. Our systematic studies on the effect of thickness of the base film suggest that there exists a thickness threshold at around 1 mm that separates the wrinkling mechanics into two regimes. When the films are thinner than 1 mm, wrinkles with many defects are formed, whose average periodicity decreases continuously as the film thickness increases to 1 mm. When the film thickness is above 1 mm, the periodicity of formed wrinkles approaches a constant value, which is independent of the film thickness and can be precisely predicted by the classical nonlinear finite mechanics. This thickness-dependent wrinkling behavior was not discovered in previous experimental and theoretical studies, so this study provides a complete understanding of the wrinkling mechanism. By conveniently controlling the thickness of the base film, we have developed robust and versatile strategies to prepare mechanochromic films with either pre-designed colorimetric responses or transparency changes depending on the film thickness. These stimuli-responsive optical properties have promising applications in anti-counterfeiting, information encryption, sensors, smart optical devices, and soft robotics.

2 Experimental

Fabrication of PDMS Films and Plasma Treatment: PDMS films were cured by aging the mixture of silicone elastomer base and curing agent. They were firstly mixed thoroughly in a typical culture plate with a mass ratio of 10:1(base to curing agent). The trapped bubbles inside were removed under vacuum for ~1 hour. Then, they were cured in an oven at 65°C for 2 hours.

Before the plasma treatment, the PDMS film was cut into certain shapes on demand. In Stretch-Plasma, PDMS films with different thicknesses were pre-stretched to certain strain and then covered by a mask, followed by plasma treatment in a vacuum (by degassing for 5 minutes) for 15 minutes. After the plasma treatment, releasing the pre-strain gave rise to wrinkles on the rigid surface. In strategy Plasma-Stretch, PDMS films, covered by the mask as well, with different thicknesses were treated by plasma without pre-strain. The following stretching will induce wrinkles on the rigid surface due to the Poison effect. The orientation of wrinkles in Stretch-Plasma and pre-strain is perpendicular and parallel in Plasma-Stretch.

Optical microscopic images were taken by a Zeiss AXIO Image optical microscope. Reflection spectra were measured by an Ocean Optics HR 2000CG-UV-NIR spectrometer coupled with a home-made sample stage to collect reflected beams around different angles. The spectral integration time was set at 300 ms. The overall morphology and cross-section of wrinkles on the surface are characterized by scanning electron microscopy (SEM, Philips FEI XL30). Optical photos were taken by a digital camera.

The peak of reflection can be predicted by derived Bragg's Law based on geometry shown in Figure 2e. During reflection measurement, the incident angle (angle between the incident light and normal) was set at 65o. Consequently, the angle between incident light and baseline was 25°. The pathway difference between incident light was p×cos (25°), where, p is the periodicity of wrinkles (767 nm for Stretch-Plasma and 1150 nm for Plasma-Stretch). Similarly, the pathway difference between the reflected light was -p×cos(θ). The derived Bragg's Law can be presented as kλ=np(cos25-cosθ), where k is reflection order; λ is the wavelength of reflection and n is the reflective index (1 for air). The dependence of the periodicity of wrinkles on the applied strain can be predicted by the nonlinear finite mechanics. It takes the effect of strain on the wavelength (P) and amplitude (A) of wavy deformation into consideration with the following formulas:

$$P = \frac{\pi h(1+\varepsilon_{applied})}{(1+\varepsilon_{pre})(1+\varepsilon_{applied}+\zeta)^{\frac{1}{3}}\sqrt{\varepsilon_c}} \quad (1)$$

$$A = h\frac{\sqrt{\frac{(\varepsilon_{pre}-\varepsilon_{applied})}{\varepsilon_c}-1}}{\sqrt{1+\varepsilon_{pre}}(1+\varepsilon_{applied}+\zeta)^{\frac{1}{3}}} \quad (2)$$

where

$$\zeta = \frac{5(\varepsilon_{pre}-\varepsilon_{applied})(1+\varepsilon_{pre})}{32}$$

$$\varepsilon_c = \frac{1}{4}\left[\frac{3E_s(1-v_f^2)}{E_f(1-v_{fs}^2)}\right]^{2/3}$$

Here h is the film thickness; E_s (2.0 MPa) and E_f (75 GPa) denote the elastic modulus of the substrate and the film, respectively while v_s (0.48) and v_f (0.27) are Poisson ratios of substrate and film. The ε_{pre} is the strain of PDMS before plasma treatment (0% for Plasma-Stretch and 12% for Stretch-Plasma) and $\varepsilon_{applied}$ is the strain applied to PDMS after plasma treatment (0 to 20% for Plasma-Stretch and 0 to 12% for Stretch-Plasma). The thickness of the oxidized layer on PDMS can be calculated by Equation 1 in the scenario of Stretch-Plasma with ε_{pre}=12%, $\varepsilon_{applied}$=0%, and P=767 nm. By substituting the calculated value of h into Equation 2, we can derive the theoretical value of the amplitude of wrinkles under the same scenario. For the dependence of periodicity of wrinkles on $\varepsilon_{applied}$ in the range of 0% to 12%, the periodicity of wrinkles at 0% is set at starting point and others can be calculated by Equation 1.

3 Results and Discussion

In a typical bilayer film, wrinkles are formed due to the contrast of elastic modulus between the top rigid layer and the bottom elastic substrate.[13] In the case of plasma-treated PDMS films, the top PDMS is oxidized into silica oxides, which have much higher elastic modulus (75 GPa) than the bottom bulk PDMS substrate (2.0 MPa). Therefore, when a plasma-treated PDMS film is subjected to external compression, the strain on the oxide layer is smaller than that on the bottom elastic substrate and the interfacial stress will be released by forming wrinkles on the surface. In this work, two methods were used to reduce wrinkles on PDMS films by changing the plasma treatment and stretching sequences. We observed similar wrinkling behaviors on the two types of PDMS films but with different wrinkle orientations with respect to the stretching direction.

3.1 Thickness-Dependent Wrinkling Behaviors

The two strategies to induce wrinkles in PDMS films are illustrated in Figure 1. In Strategy I (Figure 1a), PDMS films with different thicknesses were pre-stretched (pre-strain=12%) and then treated by oxygen plasma in a vacuum chamber (Stretch-Plasma). In strategy II (Figure 1b), PDMS films were first treated by plasma and then subjected to mechanical strains (Plasma-Stretch). Due to the formation of a rigid oxide layer on the surface of the PDMS film, both strategies can induce one dimensional (1D) wrinkles but with different orientations.[39-41] In strategy I, when the pre-strain was removed, the films relaxed to their original length. In principle, the deformation of the top rigid oxide layer is smaller than that of the soft PDMS substrates because of the high elastic modulus of the top layers. As a result, the interfacial strains between them induce the formation of wrinkles, whose orientation is perpendicular to the strains. In the second strategy, the formed wrinkles were parallel to the stretching directions due to the Poisson effect-induced shrinkage along the lateral directions. Accordingly to the previous report and theoretical studies, the thickness of the oxide layers can be controlled by treatment parameters, such as exposure time, plasma strength,

as well as the oxygen content of the surrounding.[22, 42] Typically in literature,[20] the treatment process was carried out in oxygen or airflow in a plasma chamber.

To systematically study the thickness effects in strategy I, PDMS films with different thicknesses were prepared and treated by plasma under identical conditions. As shown in Figure 2a, wrinkles formed on thick PDMS films were very uniform with well-defined long-range order, with a periodicity of ~800 nm under a pre-strain of 12%. When the thickness decreased (t < 1 mm), the formed wrinkles became larger and nonuniform. The waveform of the wrinkles was nonuniform along both the wave propagation and lateral directions. The scanning electron microscope (SEM) images of PDMS films with a thickness of 3.05 mm after the Stretch-Plasma process are shown in Figure 2b. The periodicity was measured to be 767 nm, which was very close to the value measured from optical microscopy images (783 nm). The SEM image of the cross-section of the film reveals perfect sinusoidal function shape with an amplitude of 71 nm, which is consistent with the calculated value (79.8 nm). The thickness of the silicon oxide layer was calculated to be 5.64 nm for a 3.05 mm-thick film after the Stretch-Plasma strategy. Compared with the values in previous reports.[17, 42-46] the smaller thickness of the oxide layer is reasonable since air rather than pure oxygen was introduced during plasma treatment. By carefully measuring the periodicity using optical microscopy, we found that it decreased dramatically as the thickness of PDMS films increased to 1 mm (Figure 2c). For thick PDMS films (>1 mm), however, the periodicity approached a minimum value and remained almost constant. The thickness-dependent wrinkling behaviors can be attributed to the existence of an energy threshold to induce highly ordered wrinkles in classical wrinkling mechanics. Essentially, the film wrinkling is driven by the elastic potential energy obtained during stretching, which increases with the thickness of the PDMS films. When this energy is larger than the minimum energy in the wrinkled bilayers, the wrinkling behavior (wavelength and amplitude) can be well described by the classical wrinkling mechanics. If it is lower than the minimum energy, however, the classical wrinkling mechanics can no longer describe the wrinkling behavior because its derivation is based on energy minimization of wrinkled bilayers and the energy transfer between original flat states and wrinkled states are not taken into consideration. In addition, the elastic potential energy in thin PDMS films is too small to drive the formation of uniform, relatively small wrinkles. As a result, nonuniform wrinkles with unpredictable large periodicity occur in the plasma-treated thin PDMS films.

3.2 Mechanochromic Responses

Based on the thickness-dependent wrinkling of PDMS films, we then systematically studied the mechanochromic response of the prepared films under different strains. The thick wrinkled films exhibited strong structural colors due to the constructive interference of light at the highly ordered wrinkles (Figure 2d). Instead, only random scattering was observed in thin films due to the formation of large and nonuniform wrinkles. Therefore, the PDMS film became translucent after the pre-strain was released (Figure 2d). For films prepared by strategy I, the reflected light was viewing-angle dependent as shown in the digital photos in Figure 2d. Once the incident angle was fixed, different colors from blue to red were observed at different viewing angles (supporting video 1). The thin films only became translucent at different viewing angles due to the lack of long-range orders (Figure S-1 in ESM). Notably, by simply applying a mask, we could print pre-designed patterns and images that exhibited strong structural colors while the other parts remained transparent (Figure S-2 in ESM).

The dependence of wavelength of reflected light on the detection angle can be precisely predicted by the Bragg's Law (Figure 2e).[47, 48] The pathway difference of two neighboring incident and reflected beams is highlighted as red-dashed and blue-dashed lines, respectively. Based on the incident geometry and ray optics, the light pathway differences for the incident and reflected beams that occur on two neighboring wrinkles can be derived as d*cos25 and d*cosθ, respectively. Then, the derived Bragg's equation can be described by $k\lambda=nd(\cos 25-\cos\theta)$, where k is the reflection order, λ is the wavelength of incident light, n is the refractive index of the medium (n=1 for air), d is the periodicity of wrinkles on the surface of PDMS films, and θ is the detection angle. Constructive or destructive interference occurs when

k is an integer or half-integer, respectively. Based on the derived Bragg's Law and d values (767 nm for Stretch-Plasma) measured by SEM images (Figure S-3 in ESM), the wavelength of reflection can be precisely predicted. The reflection spectra were measured based on the geometry shown in Figure 2e. The grazing angle was set as 25° and reflection spectra were collected by varying detection angle θ. As θ increased, the wavelength of reflected light had a red-shift from 250 nm (θ=55°) to 850 nm (θ=105°) in strategy I. Interestingly, we found that the reflectance had the highest intensity in the visible range, which was consistent with the brilliant structural colors on the PDMS films. Due to the high quality of wrinkles on the PDMS films, the second-order diffraction was also observed at a short wavelength, as shown in Figure 2f and highlighted in Figure S-4a in ESM. In Figure 2g and Table S-1 in ESM, the measured peak positions coincide well with the predicted values at both first and second diffraction orders. They have quasi-linear dependence on detection angle θ. In strategy II, we observed a similar thickness-dependent wrinkling behavior when the plasma-treated PDMS films were subjected to strains (Figure 3a). As shown in Figure 3b, the periodicity was 1.15 μm in strategy II with an applied strain of 20%. PDMS films without pre-strain were still transparent after plasma treatment. Mechanical strains would induce structural colors due to the formation of periodic wrinkles on the surface (Figure S-5 in ESM). In Figure 3c and Table s2, the wavelength of reflected light increased with the detection angles. Due to the larger periodicity of wrinkles in Strategy II than that in strategy I, the reflected peaks increased more dramatically with increasing θ (Figure S-4b in ESM). Such a difference in the dependence is also evidenced by the larger slope in the λ-θ curve in strategy II (Figure 3d).

To investigate how mechanical strain affects the periodicity and optical properties, we investigated the evolution of wrinkles upon post-stretching of a film prepared using Strategy I. As shown in Figure 4a, the contrast of wrinkles decreased when the strain increased, indicating the shrinkage of wave amplitude of wrinkles. Meanwhile, the density of cracking and dislocation became larger due to the mismatch between local strain and the applied strain. Therefore, the structural color on the film surface gradually disappeared when the strain increased to 12% (insets in Figure 4a). It is interesting to point out that mechanical strains could only induce a decrease in the peak intensity instead of peak shift during the stretching process (Figure 4b). The post-buckling of PDMS films, when subjected to an applied strain, could be well explained by the finite deformation mechanics and fit well with the values predicted by Equation 1. In Strategy I (ε_{pre}=12%), increasing $\varepsilon_{applied}$ from 0% to 12% leads to a 7.8% change in the periodicity and the amplitudes of wrinkles should decrease, which is consistent with our observations and measurements (Figure 4c). Such a small change in the periodicity results in a negligible shift in the peak position of the diffraction, which leads to almost invariant structural color in response to mechanical strain. For thick PDMS films treated by strategy II, they were still transparent after treatment (Figure S-6a in ESM). Mechanical strains increased the amplitude of wrinkles based on the dark-field optical microscopy images in Figure S-6a in ESM. The reflectance of thick PDMS film after plasma-stretch treatment increased gradually as the strain increased from 0% to 20% (Figure S-6b and S-6c in ESM). Post-strains induce the decreases or increases in the amplitude of wrinkles in Strategy I and II, respectively. And, no noticeable shift in reflection was observed upon different post-strains. The optical microscopy images of PDMS films after Stretch-Plasma (Figure 5a) reveal that the amplitude of wrinkles decreased as the applied strain increased, which reduced the scattering of light on the surface. As a result, the pattern on the surface disappeared gradually (insets in Figure 5a) and the transmittance increased accordingly (Figure 5b and 5c). In the Plasma-Stretch process, however, the dependence is the opposite. Stretching increased the amplitude of wrinkles and the pattern became more translucent (Figure S-6d and S-6e in ESM). The transition of microstructures and consequent development in optical properties are highly reversible. The original states will recover by simply releasing the applied strains, which can be observed in supporting Video 2. Based on the controllable optical properties of PDMS films and the flexible preparation processes, we further demonstrate that the thickness-dependent wrinkling of PDMS films can be used to prepare smart optical devices with desirable mechanochromic

responses. By simply applying a mask, we created arbitrary images on the surface of PDMS films. As shown in Figure 6a, a complex pattern was printed on the surface of a PDMS film using the Plasma-Stretch strategy. Upon stretching, the transparent PDMS film exhibited brilliant and uniform structural colors. Thanks to the photomask, only the exposed areas were oxidized by plasma, giving rise to well-defined patterns under external strains. The created images showed different colors by varying the viewing angles. The transition was quite sensitive and quick (See supporting Video 3). For a thin PDMS film, it became translucent under applied strains (Figure 6b). In Figure 6c, three letters were printed on a thick PDMS film using the Stretch-Plasma strategy with the help of commercial stencils. They exhibited different colors under various illumination conditions as well as different viewing angles. The scheme on the left of Figure 6c illustrates how those pictures were taken. Interestingly, there were color gradients if a point light was applied (Figure 6d). This phenomenon is typical in structural colors based on Bragg's theorem due to the variance in the pathway difference of incident light. On the other hand, if the patterns were illuminated by directional light, uniform monochrome patterns were observed and could be tuned continuously across the visible range from blue to red by lowing the viewing angle (Figure 6e). This effect could be ascribed to the increasing pathway difference and subsequently red-shift of the reflected peak. Figure 7a demonstrates the complementary and reversible coloration process by sequentially treating PDMS films with strain and plasma. The first and second plasma treatments were run with and without strain and mask, respectively. In a typical process, the PDMS substrate was first stretched along its length and plasma treatment was carried out under a commercial mask. When the pre-strain was released, uniform wrinkles were formed with perpendicular alignment to the stretching direction. Therefore, a positive pattern could be observed under incident plane 1 (Figure 7b). The uniform colors indicate the high quality of orders on a large length scale. During the second plasma treatment, the mask was removed and PDMS was treated by the same condition as the first treatment. In this process, the remaining surface of the PDMS substrate was oxidized to form a thin, rigid film. When the film was subject to the pre-strain again, the patterns that were formed in the first plasma treatment disappeared. Meanwhile, uniform wrinkles were formed with the same alignment to the stretching direction at the areas that were treated by the second plasma. As a result, a negative pattern came into view gradually in incident plane 2 (Figure 7c).

4. Conclusions

In summary, we report a remarkable thickness-dependent wrinkling behavior of PDMS films by using the typical Stretch-Plasma and Plasma-Stretch processes. This nonlinear dependence of wrinkling on substrate thickness originates from a barrier for the perturbation energy in the derivation of the classic nonlinear finite mechanics and hence separates the wrinkling mechanics into two regimes. For thick PDMS films, uniform wrinkles with periodicity comparable to the wavelength of visible light were formed when the plasma-treated PDMS films were subjected to interfacial strains. In this regime, the wrinkles formation can be precisely predicted by the classic nonlinear finite mechanics. In the case of thin PDMS films, the formed wrinkles were nonuniform with lots of dislocations. And, it was found that the periodicity of wrinkles decreased as the film thickness increased in the second regime. Based on these new understandings, we have achieved brilliant structural colors and pre-designed colorimetric responses to mechanical stimuli on plasma-treated PDMS films by controlling the substrate thickness. Owing to the high-quality order of the wrinkles and their considerably small size, bright and uniform structural colors with angle-dependent properties were observed on thick PDMS films (>1 mm). For thin PDMS films, only a translucent-transparent transition was observed, whose transmittance could be tuned by applied strains. Thanks to these unique thickness-dependent optical properties, we have developed several intriguing mechanochromic devices via the flexible stretch-plasma treatment. Various patterns could be easily printed on PDMS films. The thickness-dependent and mechano-responsive optical properties are expected to further diversify the potential applications of bilayer films in anti-counterfeiting devices, smart windows, wearable electronic devices, display, and pressure sensors.

Acknowledgements

We are grateful for the financial support from the U.S. National Science Foundation (DMR-1810485).

Electronic Supplementary Material: Supplementary material (further details of the optical microscopic images, SEM images, and Reflection spectrum measurements) is available in the online version of this article at http://dx.doi.org/10.1007/10.1007/s12274-***-****-* (automatically inserted by the publisher) and is accessible free of charge

References:

[1] Bowden, N.; Brittain, S.; Evans, A. G.; Hutchinson, J. W.; Whitesides, G. M. Spontaneous formation of ordered structures in thin films of metals supported on an elastomeric polymer. *Nature* **1998,** *393*, 146-149.

[2] Yu, C.; O'Brien, K.; Zhang, Y.-H.; Yu, H.; Jiang, H. Tunable optical gratings based on buckled nanoscale thin films on transparent elastomeric substrates. *Appl. Phys. Lett.* **2010,** *96*, 041111.

[3] Ma, T.; Liang, H.; Chen, G.; Poon, B.; Jiang, H.; Yu, H. Micro-strain sensing using wrinkled stiff thin films on soft substrates as tunable optical grating. *Opt. Express* **2013,** *21*, 11994-12001.

[4] Li, Z.; Yang, D.; Liu, X.; Ma, H. Substrate-induced controllable wrinkling for facile nanofabrication. *Macromol. Rapid Commun.* **2009,** *30*, 1549-1553.

[5] Khang, D.-Y.; Jiang, H.; Huang, Y.; Rogers, J. A. A stretchable form of single-crystal silicon for high-performance electronics on rubber substrates. *Science* **2006,** *311*, 208-212.

[6] Jiang, H.; Khang, D.-Y.; Song, J.; Sun, Y.; Huang, Y.; Rogers, J. A. Finite deformation mechanics in buckled thin films on compliant supports. *Proc. Natl. Acad. Sci. U.S.A.* **2007,** *104*, 15607-15612.

[7] Song, J.; Jiang, H.; Choi, W.; Khang, D.; Huang, Y.; Rogers, J. An analytical study of two-dimensional buckling of thin films on compliant substrates. *J. Appl. Phys.* **2008,** *103*, 014303.

[8] Choi, W. M.; Song, J.; Khang, D.-Y.; Jiang, H.; Huang, Y. Y.; Rogers, J. A. Biaxially stretchable "wavy" silicon nanomembranes. *Nano Lett.* **2007,** *7*, 1655-1663.

[9] Wang, Y.; Yang, R.; Shi, Z.; Zhang, L.; Shi, D.; Wang, E.; Zhang, G. Super-elastic graphene ripples for flexible strain sensors. *ACS Nano* **2011,** *5*, 3645-3650.

[10] Chae, S. H.; Yu, W. J.; Bae, J. J.; Duong, D. L.; Perello, D.; Jeong, H. Y.; Ta, Q. H.; Ly, T. H.; Vu, Q. A.; Yun, M. Transferred wrinkled al2o3 for highly stretchable and transparent graphene–carbon nanotube transistors. *Nature Mater.* **2013,** *12*, 403-409.

[11] Zang, J.; Ryu, S.; Pugno, N.; Wang, Q.; Tu, Q.; Buehler, M. J.; Zhao, X. Multifunctionality and control of the crumpling and unfolding of large-area graphene. *Nature Mater.* **2013,** *12*, 321-325.

[12] Chen, T.; Xue, Y.; Roy, A. K.; Dai, L. Transparent and stretchable high-performance supercapacitors based on wrinkled graphene electrodes. *ACS Nano* **2013,** *8*, 1039-1046.

[13] Stafford, C. M.; Harrison, C.; Beers, K. L.; Karim, A.; Amis, E. J.; VanLandingham, M. R.; Kim, H.-C.; Volksen, W.; Miller, R. D.; Simonyi, E. E. A buckling-based metrology for measuring the elastic moduli of polymeric thin films. *Nature Mater.* **2004,** *3*, 545.

[14] Stafford, C. M.; Vogt, B. D.; Harrison, C.; Julthongpiput, D.; Huang, R. Elastic moduli of ultrathin amorphous polymer films. *Macromolecules* **2006,** *39*, 5095-5099.

[15] Chung, J. Y.; Chastek, T. Q.; Fasolka, M. J.; Ro, H. W.; Stafford, C. M. Quantifying residual stress in nanoscale thin polymer films via surface wrinkling. *Acs Nano* **2009,** *3*, 844-852.

[16] Wilder, E. A.; Guo, S.; Lin-Gibson, S.; Fasolka, M. J.; Stafford, C. M. Measuring the modulus of soft polymer networks via a buckling-based metrology. *Macromolecules* **2006,** *39*, 4138-4143.

[17] Yu, C.; Jiang, H. Forming wrinkled stiff films on polymeric substrates at room temperature for stretchable interconnects applications. *Thin Solid Films* **2010,** *519*, 818-822.

[18] Huck, W. T. Artificial skins: Hierarchical wrinkling. *Nature Mater.* **2005,** *4*, 271-272.

[19] Cai, S.; Breid, D.; Crosby, A. J.; Suo, Z.; Hutchinson, J. W. Periodic patterns and energy states of buckled films on compliant substrates. *J. Mech. Phys. Solids* **2011,** *59*, 1094-1114.

[20] Kim, P.; Hu, Y.; Alvarenga, J.; Kolle, M.; Suo, Z.; Aizenberg, J. Rational design of mechano-responsive optical materials by fine tuning the evolution of

strain‐dependent wrinkling patterns. *Adv. Opt. Mater.* **2013,** *1*, 381-388.
[21] Hanske, C.; Tebbe, M.; Kuttner, C.; Bieber, V.; Tsukruk, V. V.; Chanana, M.; König, T. A.; Fery, A. Strongly coupled plasmonic modes on macroscopic areas via template-assisted colloidal self-assembly. *Nano Lett.* **2014,** *14*, 6863-6871.
[22] Nania, M.; Matar, O. K.; Cabral, J. T. Frontal vitrification of pdms using air plasma and consequences for surface wrinkling. *Soft matter* **2015,** *11*, 3067-3075.
[23] Hou, H.; Yin, J.; Jiang, X. Smart patterned surface with dynamic wrinkles. *Acc. Chem. Res.* **2019,** *52*, 1025-1035.
[24] Melzer, M.; Karnaushenko, D.; Lin, G.; Baunack, S.; Makarov, D.; Schmidt, O. G. Direct transfer of magnetic sensor devices to elastomeric supports for stretchable electronics. *Adv. Mater.* **2015,** *27*, 1333-1338.
[25] Quereda, J.; San-Jose, P.; Parente, V.; Vaquero-Garzon, L.; Molina-Mendoza, A. J.; Agraït, N.; Rubio-Bollinger, G.; Guinea, F.; Roldán, R.; Castellanos-Gomez, A. Strong modulation of optical properties in black phosphorus through strain-engineered rippling. *Nano Lett.* **2016,** *16*, 2931-2937.
[26] Xie, T.; Xiao, X.; Li, J.; Wang, R. Encoding localized strain history through wrinkle based structural colors. *Adv. Mater.* **2010,** *22*, 4390-4394.
[27] Ohzono, T.; Suzuki, K.; Yamaguchi, T.; Fukuda, N. Tunable optical diffuser based on deformable wrinkles. *Adv. Opt. Mater.* **2013,** *1*, 374-380.
[28] Li, Z.; Yin, Y. Stimuli‐responsive optical nanomaterials. *Adv. Mater.* **2019,** *31*, 1807061.
[29] Bae, H. J.; Bae, S.; Park, C.; Han, S.; Kim, J.; Kim, L. N.; Kim, K.; Song, S. H.; Park, W.; Kwon, S. Biomimetic microfingerprints for anti‐counterfeiting strategies. *Adv. Mater.* **2015,** *27*, 2083-2089.
[30] Choi, H.; Kim, J.; Lee, H.; Song, S.; Han, J.; Moon, M. Wrinkle-based measurement of elastic modulus of nano-scale thin pt film deposited on polymeric substrate: Verification and uncertainty analysis. *Exp. Mech.* **2010,** *50*, 635-641.
[31] Huang, Z.; Hong, W.; Suo, Z. Nonlinear analyses of wrinkles in a film bonded to a compliant substrate. *J. Mech. Phys. Solids* **2005,** *53*, 2101-2118.
[32] Huang, R.; Suo, Z. Wrinkling of a compressed elastic film on a viscous layer. *J. Appl. Phys.* **2002,** *91*, 1135-1142.
[33] Huang, R. Kinetic wrinkling of an elastic film on a viscoelastic substrate. *J. Mech. Phys. Solids* **2005,** *53*, 63-89.
[34] Im, S.; Huang, R. Evolution of wrinkles in elastic-viscoelastic bilayer thin films. *J. Appl. Mech.* **2005,** *72*, 955-961.
[35] Chen, X.; Hutchinson, J. W. Herringbone buckling patterns of compressed thin films on compliant substrates. *J. Appl. Mech.* **2004,** *71*, 597-603.
[36] Groenewold, J. Wrinkling of plates coupled with soft elastic media. *Physica A.* **2001,** *298*, 32-45.
[37] Huang, R.; Suo, Z. Instability of a compressed elastic film on a viscous layer. *Int. J. Solids Struc.* **2002,** *39*, 1791-1802.
[38] Huang, R.; Yin, H.; Liang, J.; Sturm, J.; Hobart, K.; Suo, Z. Mechanics of relaxing sige islands on a viscous glass. *Acta Mech. Sinica* **2002,** *18*, 441-456.
[39] Mirley, C.; Koberstein, J. A room temperature method for the preparation of ultrathin siox films from langmuir-blodgett layers. *Langmuir* **1995,** *11*, 1049-1052.
[40] Chan, V. Z.-H.; Thomas, E. L.; Frommer, J.; Sampson, D.; Campbell, R.; Miller, D.; Hawker, C.; Lee, V.; Miller, R. D. Curious morphology of silicon-containing polymer films on exposure to oxygen plasma. *Chem. Mater.* **1998,** *10*, 3895-3901.
[41] Bodas, D.; Khan-Malek, C. Formation of more stable hydrophilic surfaces of pdms by plasma and chemical treatments. *Microelectron. Eng.* **2006,** *83*, 1277-1279.
[42] Bayley, F. A.; Liao, J. L.; Stavrinou, P. N.; Chiche, A.; Cabral, J. T. Wavefront kinetics of plasma oxidation of polydimethylsiloxane: Limits for sub-μm wrinkling. *Soft matter* **2014,** *10*, 1155-1166.
[43] Ouyang, M.; Yuan, C.; Muisener, R.; Boulares, A.; Koberstein, J. Conversion of some siloxane polymers to silicon oxide by uv/ozone photochemical processes. *Chem. Mater.* **2000,** *12*, 1591-1596.
[44] Owen, M. J.; Smith, P. J. Plasma treatment of polydimethylsiloxane. *J. Adhes. Sci. Technol.* **1994,** *8*, 1063-1075.
[45] Hillborg, H.; Gedde, U. Hydrophobicity recovery of polydimethylsiloxane after exposure to corona discharges. *Polymer* **1998,** *39*, 1991-1998.
[46] Béfahy, S.; Lipnik, P.; Pardoen, T.; Nascimento, C.; Patris, B.; Bertrand, P.; Yunus, S. Thickness and elastic modulus of plasma treated pdms silica-like surface layer. *Langmuir* **2009,** *26*, 3372-3375.

[47] Li, Z.; Yang, F.; Yin, Y. Smart materials by nanoscale magnetic assembly. *Adv. Funct. Mater.* **2019**, 1903467.
[48] Li, Z.; Wang, M.; Zhang, X.; Wang, D.; Xu, W.; Yin, Y. Magnetic assembly of nanocubes for orientation-dependent photonic responses. *Nano Lett.* **2019,** *19*, 6673-6680.

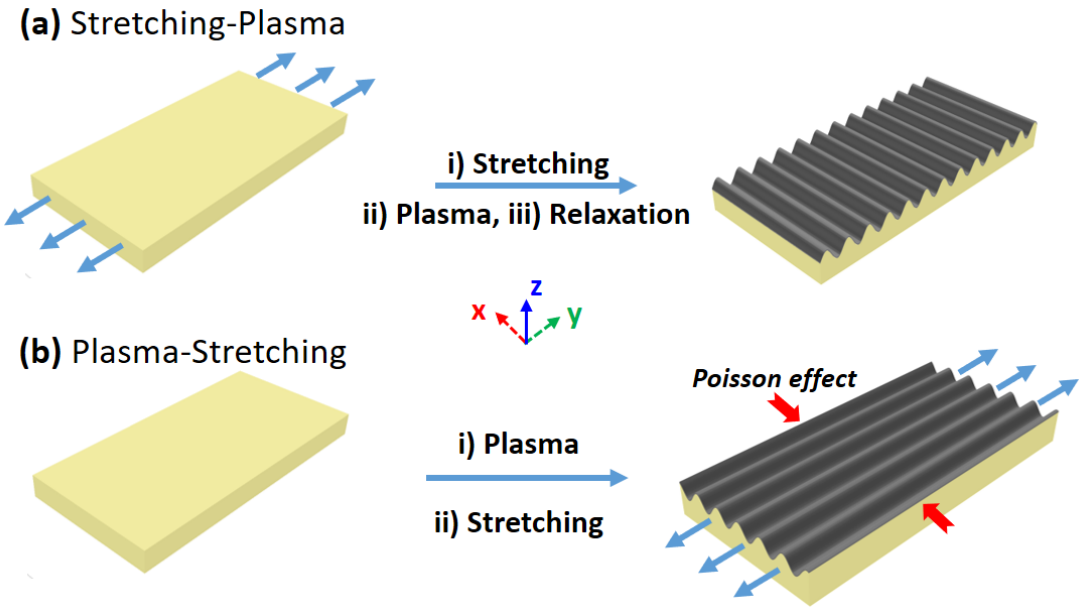

Figure 1. Schematic illustration of the fabrication processes. a). PDMS films with different thicknesses are pre-stretched and then treated by plasma.The release of pre-strain will induce wrinkles, which are perpendicular to the direction of pre-strain. b). PDMS films are firstly treated with plasma and then stretched, which will induce parallel wrinkles to the strain direction due to the Poisson effect.

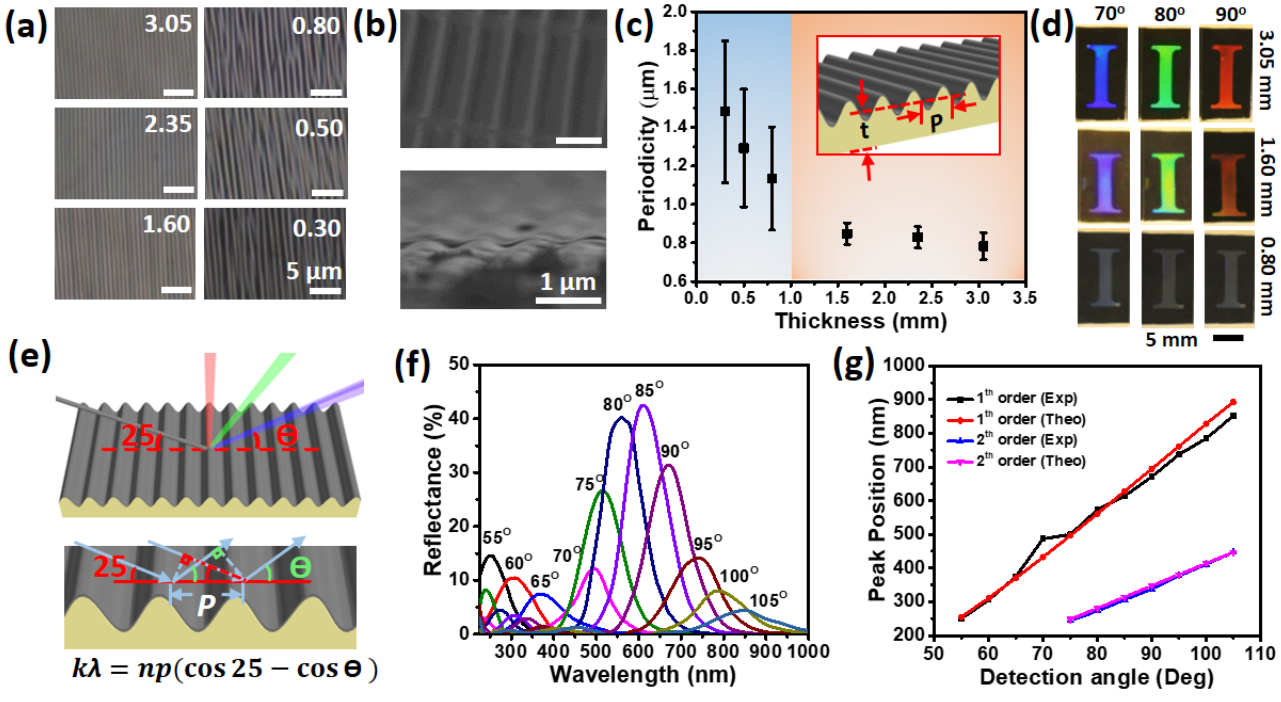

Figure 2. a) Optical microscopy images of PDMS films after Stretch-Plasma. b) SEM images of a thick (3.05mm) PDMS film and cross-section (bottom). c) Dependence of averaged periodicity on the thickness of PDMS films. d) Digital images of PDMS films with different thicknesses and viewing angles. e) Illustration of geometry for reflectance measurement (top) and numerical calculation (bottom). f) Reflectance of PDMS films measured by varying Θ shown in (e) (bottom). g) Dependence of peak position on detection angle Θ. PDMS film was treated by Stretch-Plasma. The thickness of PDMS film in (f) is 3.05 mm.

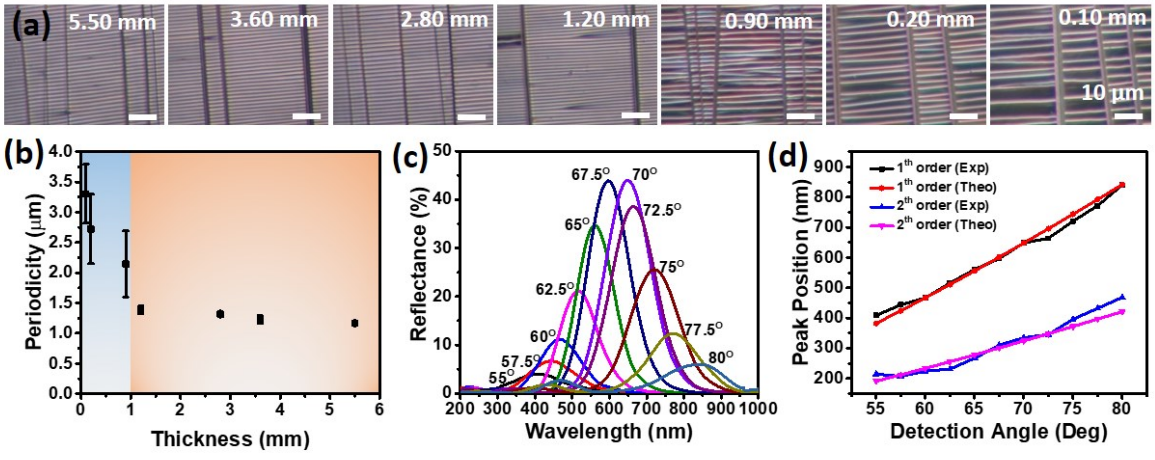

Figure 3. a) Optical microscopy images of PDMS films of different thicknesses under a strain of 20%. b) Dependence of averaged periodicity on the thickness of PDMS films. c) The reflectance of a PDMS film measured by varying Θ. d) Dependence of peak position on detection angle Θ. PDMS film was treated by Plasma-Stretch. The thickness of PDMS film in (b) is 3.60 mm.

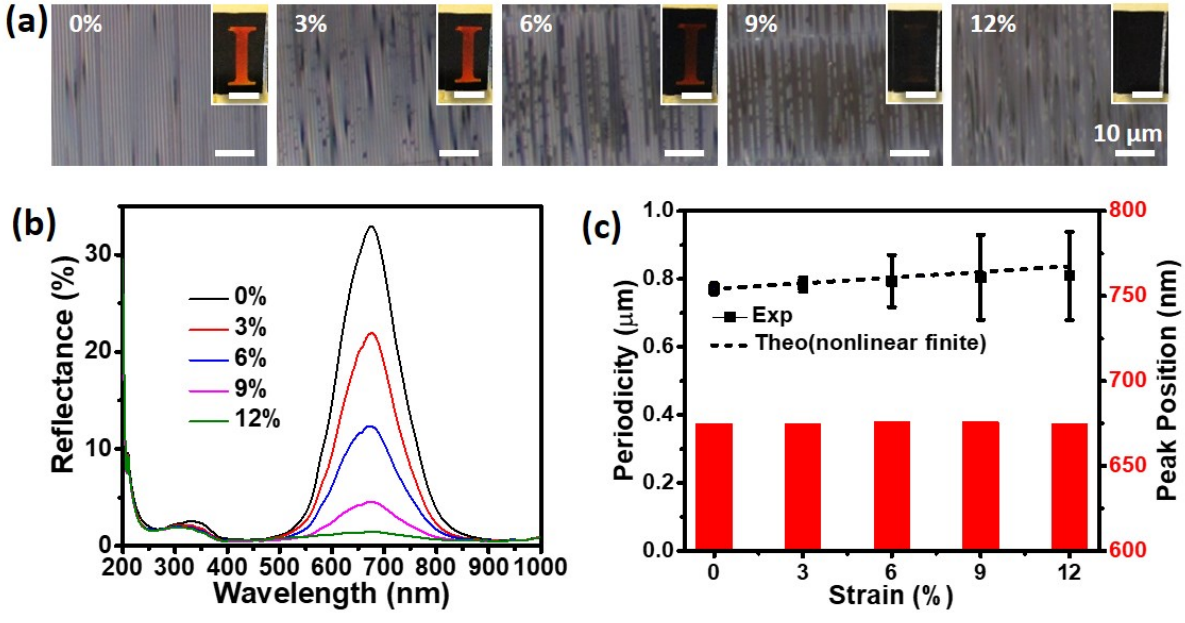

Figure 4. Mechanochromic properties of a PDMS film after Stretch-Plasma treatment. a) Optical microscopy images of a thick (3.05mm) PDMS film. Insets illustrate the optical transitions of the PDMS film at different stretching stages. Scale bars in insets: 5 mm. (b) Mechano-responsive reflectance of the PDMS film. c). Dependence of periodicity and peak positions of reflection on applied strains. The predicted values of periodicity are plotted in c based on nonlinear finite mechanics (See numerical calculation in the experimental section).

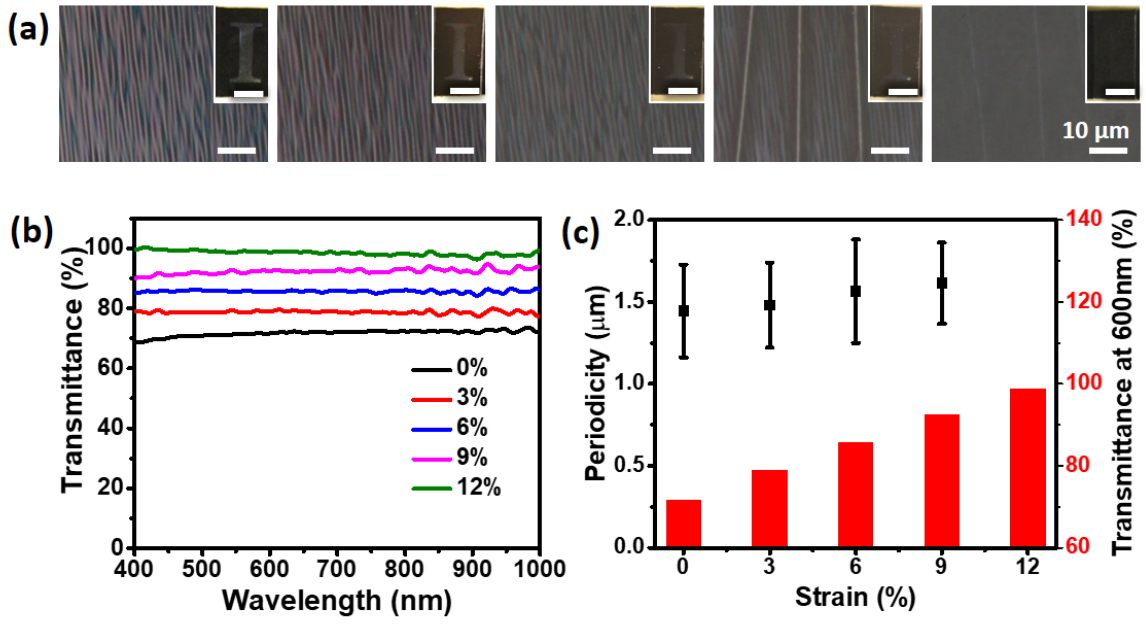

Figure 5. Mechano-responsive optical properties of PDMS films after Stretch-Plasma treatment. a) Optical microscopic images of thin (0.30mm) PDMS. Inset illustrates the optical transitions of PDMS films at different stretching stages. Scale bars in insets: 5 mm. (b) Mechano-responsive transmittance of the PDMS film. c) Dependence of periodicity and transmittance of the thin PDMS film on applied strains.

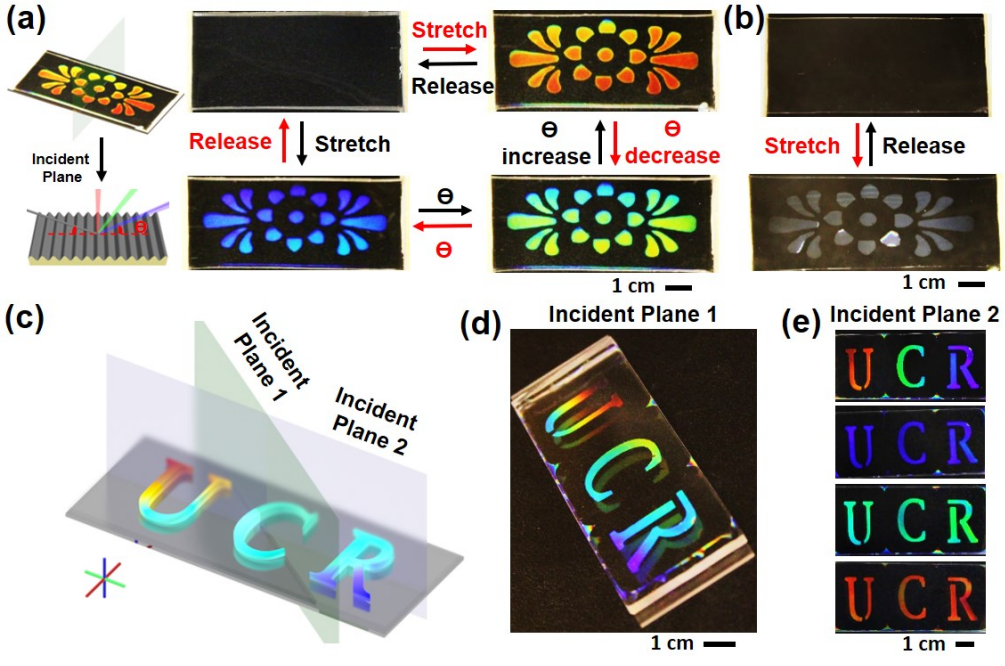

Figure 6. Flexible fabrication processes for encryption and mechanochromic films. Photos of thick (a) and thin (b) PDMS films under Plasma-Stretch treatment. Images were taken according to the geometry in (a). c) Schematic illustration of the PDMS under Stretch-Plasma treatment. d) Photo of a PDMS film after releasing the pre-strain, which was taken in the incident plane 1 under point light source. e) Photo of the PDMS film taken in the incident plane 2 after releasing the pre-strain.

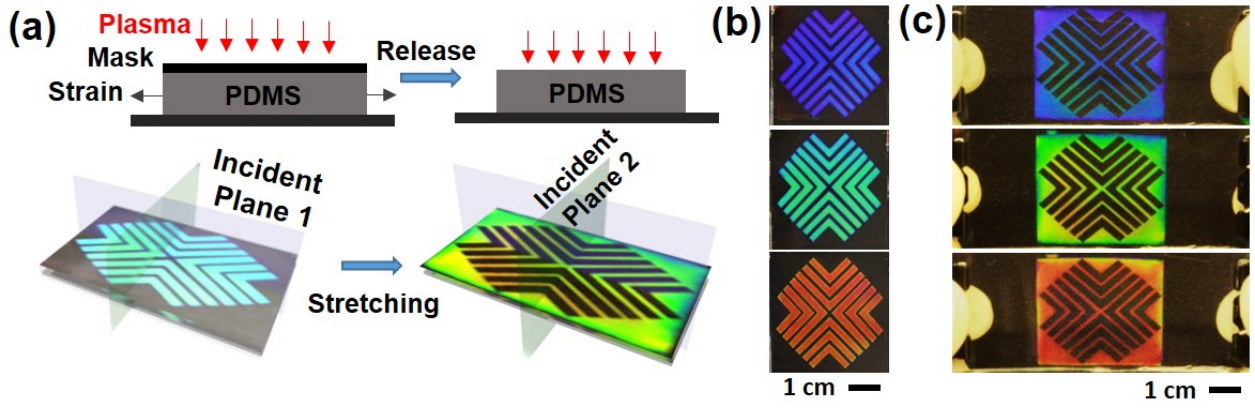

Figure 7. The combination of plasma treatment and stretch gives rise to complementary mechanochromic response and information encryption. a) Fabrication process and schemes illustrating the complementary and reversible coloration-discoloration transition. b) Photos of the fabricated PDMS film taken in the incident plane 1 right after releasing the pre-strain. c) Photos of the same PDMS film taken in the incident plane 2 when subjected to additional stretching along the length of the film. The viewing angle (Θ) from top to bottom increased. For all patterns and letters on thick PDMS film, structural colors were dependent on viewing angles.